CHEMISTRY
A European Journal

A Journal of
ChemPubSoc Europe

Accepted Article

Title: PIDAZTA: Structurally Constrained Chelators for Efficient Formation of Stable Gallium-68 Complexes at Physiological pH

Authors: Giovanni Battista Giovenzana, Edit Farkas, Adrienn Vágner, Roberto Negri, Luciano Lattuada, Imre Tóth, Valentina Colombo, David Esteban-Gómez, Carlos Platas-Iglesias, Johannes Notni, and Zsolt Baranyai

To be cited as: *Chem. Eur. J.* 10.1002/chem.201901512

Link to VoR: http://dx.doi.org/10.1002/chem.201901512

Supported by
ACES

WILEY-VCH

10.1002/chem.201901512

WILEY-VCH

PIDAZTA: Structurally Constrained Chelators for Efficient Formation of Stable Gallium-68 Complexes at Physiological pH

Edit Farkas,[a] Adrienn Vágner,[a] Roberto Negri,[b] Luciano Lattuada,[c] Imre Tóth,[a][d] Valentina Colombo,[e] David Esteban-Gómez,[f] Carlos Platas-Iglesias,[f] Johannes Notni,*[g] Zsolt Baranyai,*[a][c] and Giovanni B. Giovenzana,*[b]

Dedicated to Prof. Silvio Aime in occasion of his 70th birthday

Abstract: Two structurally constrained chelators based on a fused bicyclic scaffold, [(4*R**,10a*S**)-PIDAZTA (L1) and (4*R**,10a*R**)-PIDAZTA (L2)], were designed for the preparation of Ga^{III}-based radiopharmaceuticals. The stereochemistry of the ligand scaffold has a deep impact on the properties of the complexes, with unexpected [Ga(L2)OH] species being superior in terms of both thermodynamic stability and inertness. This peculiar behavior was rationalized on the basis of molecular modeling and appears to be related to a better fit in size of Ga^{III} into the cavity of L2. Fast and efficient formation of the Ga^{III}-chelates at room temperature was observed at pH values between 7 and 8, which enables ^{68}Ga radiolabeling under truly physiological conditions (pH 7.4).

Introduction

There are two radioisotopes of gallium which are practically available for clinical application. While the γ-emitter ^{67}Ga ($t_{1/2}$ = 78.3 h) only plays a subordinate role for scintigraphy, the clinical use of the positron emitter ^{68}Ga ($t_{1/2}$ = 67.7 min) has seen a particularly strong increase within the last decade.[1] The broad commercial availability of $^{68}Ge/^{68}Ga$ generators (small benchtop devices providing $^{68}Ga^{III}$ in form of its hexaaqua complex in dilute HCl)[2] and the high clinical value of some ^{68}Ga-labelled positron emission tomography (PET) radiopharmaceuticals, above all, somatostatin analogs and prostate-specific membrane antigen inhibitors, have firmly established ^{68}Ga in clinical nuclear medicine. [3]

[a] Dr. E. Farkas, Dr. A. Vagner, Prof. I. Toth, Dr. Zs. Baranyai, Dept. of Inorganic and Analytical Chemistry University of Debrecen, H-4010, Debrecen, Egyetem tér 1., Hungary
[b] Dr. R. Negri, Prof. G.B. Giovenzana, Dip. di Scienze del Farmaco, Università del Piemonte Orientale, Largo Donegani 2/3, 28100 Novara, Italy. Email: giovannibattista.giovenzana@uniupo.it
[c] Dr. Zs. Baranyai, Dr. L. Lattuada, Bracco Imaging spa, Bracco Research Centre, Via Ribes 5, 10010 Colleretto Giacosa (TO), Italy. E-mail: Zsolt.Baranyai@bracco.com
[d] Prof. I Tóth, Dept. of Physical Chemistry University of Debrecen, H-4010, Debrecen, Egyetem tér 1., Hungary
[e] Dr. V. Colombo, Dip. di Chimica, Università degli Studi di Milano, Via Golgi 19, 20133 Milano, Italy
[f] Dr. D. Esteban-Gómez, Prof. C. Platas-Iglesias, Centro de Investigacións Científicas Avanzadas (CICA) and Dep. de Química, Facultade de Ciencias, Universidade da Coruña, 15071 A Coruña, Galicia, Spain
[g] Dr. J. Notni, Lehrstuhl für Pharmazeutische Radiochemie, Technische Universität München, Walther-Meißner-Strasse 3, D-85748 Garching, Germany

Supporting information for this article is given via a link at the end of the document.

The half-life of ^{68}Ga matches the pharmacokinetics of low molecular weight radiopharmaceuticals. Like other radiometal ions, the introduction of $^{67/68}Ga^{III}$ in a diagnostic vector (peptides, antibodies) does not rely on complex reaction sequences used for lighter isotopes such as ^{18}F or ^{11}C, but rather requires a suitably designed chelating agent,[4] which is covalently linked to the vector[5] and binds the radiometal by complex formation. Ideally, such a chelator shows a high affinity and selectivity for Ga^{III}, along with rapid complexation kinetics matching the short lifetime of the radionuclide and high inertness to avoid dissociation in the bio-fluids before excretion and/or radioactive decay. However, many novel Ga^{III} radiopharmaceuticals are still prepared using the well-known chelating agent DOTA (1,4,7,10-tetraazacyclododecane-1,4,7,10-tetraacetic acid), despite its slow Ga^{III} complexation kinetics which is surpassed by many other chelators, for example, its hexadentate analogue NOTA (1,4,7-triazacyclononane-1,4,7-triacetic acid) and its bifunctional derivatives,[6a] its phosphinate congener NOPO, [6b] HBED-CC, [6c] or polydentate siderophores.[6d-e] The main reason might be the broad commercial availability of a wide variety of functionalised DOTA derivatives for direct conjugation to specific vectors with established protocols.[7]

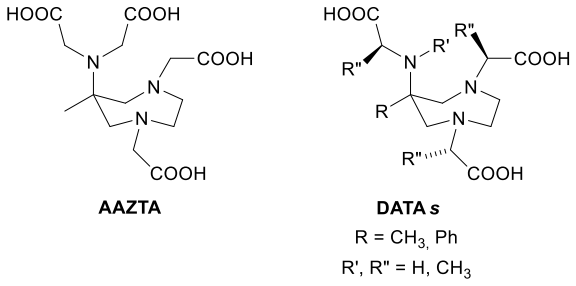

Figure 1. AAZTA and derivatives studied for Ga^{III} chelation.

In this context, the chelator AAZTA[8] (Fig. 1) was recently shown to be a highly interesting scaffold, since it quickly forms thermodynamically stable complexes with gallium(III)[9] and other ions of diagnostic interest.[10] Bifunctional derivatives of AAZTA were used in conjugates with peptides (Tyr^3-Octreotide[11] and Minigastrin[12]) and RGD-peptidomimetics[13] showing accumulation in tumours of the corresponding $^{68}Ga^{III}$-chelates, and with the bisphosphonate group for PET-imaging of bones.[14] Moreover, structural studies were devoted to shed light on the coordination behaviour of the 1,4-diazepane ring and the carboxymethyl side arms of AAZTA towards Ga^{III}. For this reason, the preparation of AAZTA derivatives with a lower

denticity, termed DATA*s*[15] (Fig. 1) and different coordinating arms[16] was reported to better understand the role of donor groups in the coordination of the classically hexacoordinated Ga^{III}. The results of the study of their coordination properties highlighted the role of the side arms (number and steric hindrance), and even more importantly, the ring substitution pattern, on the overall stability of the corresponding Ga^{III} chelates.[17,18] For example, the change from R = CH_3 to R = Ph in the structure of DATA affects the conformational population of the seven-membered ring and accordingly the affinity for the metal ion.[19,20] A careful design of the structure of the ligand is therefore crucial in the search for improved and more efficient chelating agents for Ga^{III}.

The strong affinity of AAZTA and its derivatives for Ga^{III} combined with the fast kinetics of the complex formation prompted us to explore the possibility to improve these promising properties by designing new related chelating agents. For this purpose, we have chosen to pursuit the conformational locking of the 6-amino-1,4-diazepane substructure of this family of chelating agents by ring-fusion with an additional six-membered ring. The ring-fusion was planned to include one of the coordinating nitrogen atoms, to maximise its influence on the restricted conformational freedom of the complex arising from the hexadentate chelating agent. A similar strategy was recently reported for a conformationally locked AAZTA derivative (CyAAZTA), leading to a heptadentate ligand in which the ring fusion does not directly involve coordinating atoms in any of the key bridgehead positions.[21]

In the present work, we report on the preparation of two novel isomeric chelating agents, *i.e.*: 4-amino-4-methylperhydro-pyrido[1,2-a][1,4]diazepin-*N,N′,N′*-triacetic acids, ("PIDAZTA*s*", isomers hereinafter referred to as **L1** and **L2**) depicted in Scheme 1, along with the synthetic route adopted for their preparation. We investigated thermodynamics, transmetallation kinetics and structural properties of the Ga^{III}-, Ca^{II}-, Mn^{II}-, Zn^{II}-, Cu^{II}- and Ln^{III}- complexes formed with the two PIDAZTA isomers. Furthermore, in order to elucidate their practical value for application in ^{68}Ga radiopharmaceuticals, both isomers were characterized in terms of ^{68}Ga labelling properties and kinetic inertness of the resulting radiometal complexes.

Results and Discussion

The synthesis of the chelating agents (Scheme 1) starts from commercially available (±)-2-(aminomethyl)piperidine (**1**), whose primary amino group was selectively *N*-benzylated through sequential formation of the imine by dehydrative condensation with benzaldehyde in dichloromethane, followed by reduction with $NaBH_4$ to diamine **2**. The latter was subjected to a double nitro-Mannich reaction with (para)formaldehyde and nitroethane, leading to the formation of the isomeric bicyclic nitrodiamines **3** and **4**, easily separated by column chromatography. The availability of both isomers is crucial for a comprehensive evaluation of the ring fusion influence on the resulting complexing ability towards Ga^{III}.

The identity of the isomers was assessed by single crystal X-ray diffraction analysis of nitrodiamine **3**, thus establishing its (4*R**,10a*S**) stereochemistry (Fig. S1, S2), and assigning the configuration (4*R**,10a*R**) to the diastereomeric pair **4**. Parallel treatment of the separated isomers with H_2 on Pd/C resulted in the combined hydrogenation-debenzylation leading to the triamines **5** and **6**. The introduction of the carboxymethyl side arms was achieved by an exhaustive alkylation with *t*-butyl bromoacetate in acetonitrile in the presence of K_2CO_3, followed by the removal of the *t*-butyl groups with neat TFA to obtain the desired chelating agents **L1** and **L2**, respectively.

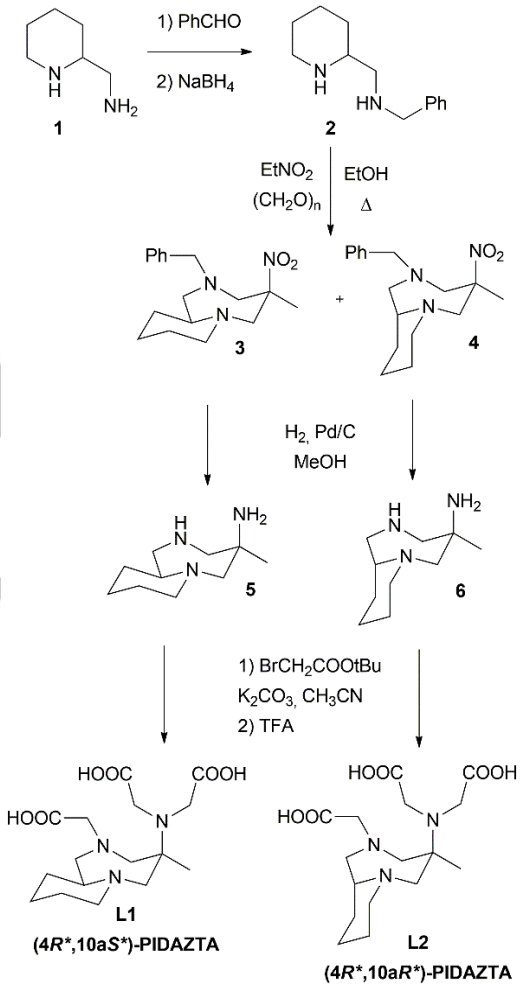

Scheme 1. Synthetic preparation of the chelating agents **L1** and **L2**.

Diffractometric analysis of a single crystal of **L1** (Fig. 2, S3, S4), grown by evaporation of a solution in methanol, confirmed the relative stereochemistry of this isomer as (4*R**,10a*S**) and its expected retention through the entire synthetic process. The compound is chiral and crystallizes in the centric space group $P2_1/c$ as a racemate, with one molecule per asymmetric unit (additional details are reported in the ESI). Fig. 2 shows the absolute configuration of the stereocentres for the arbitrary

choice of one enantiomer. In this structure, the piperidine ring is found to be in a chair conformation, whereas the seven-membered ring has a chair-like conformation. The pendant carboxylic groups are employed to set up strong H-bond contacts. Indeed, in the solid state, one *intra*-molecular H-bond of the type O-H···O (2.531 Å) is found between two pendant, carboxymethyl groups of the exocyclic iminodiacetic (IMD) residue, whereas the third carboxymethyl arm, located on the endocyclic nitrogen atom, is involved in an *inter*-molecular HB (2.603 Å) connecting the molecules in collinear chains, running in the [001] crystallographic direction (Fig. S4). **L1** is in its zwitterionic form, in which the deprotonation of one carboxylic group is observed, with concomitant protonation of the nitrogen atom involved in the ring fusion.

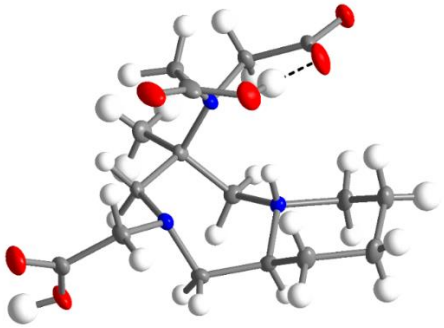

Figure 2. X-Ray structure of (4*R**,10a*S**)-PIDAZTA (**L1**). Thermal ellipsoids of non-H atoms were drawn at the 50% probability level. Intra-molecular H-bonds are depicted with dashed lines. Colour codes: O, red; N, blue; C, gray; H, white.

Solution equilibrium properties of the Ga^{3+}-L1/L2 systems

The *in vivo* application of ^{68}Ga isotope requires very robust $^{68}Ga^{III}$-complexes, which must be characterised by high thermodynamic stability and kinetic inertness in order to limit the transmetallation or transchelation reactions with competing endogenous species.[4,22-25] The stability and protonation constants of the [Ga(**L1**/**L2**)] complexes have been calculated by using the data obtained with pH-potentiometry, ^{1}H- and ^{71}Ga-NMR spectroscopy. ^{1}H- and ^{71}Ga-NMR spectra of the Ga^{III}-**L1** and Ga^{III}-**L2** systems at different pH values are reported in Fig. S7-S10. The stepwise protonation constants of the free **L1**/**L2** ligands (logK_i^H) used for the calculation of the stability and the protonation constant of [Ga(**L1**/**L2**)] complexes are reported in Table S3. The stability and protonation constants of [Ga(**L1**/**L2**)] complexes obtained by pH-potentiometry, ^{1}H- and ^{71}Ga-NMR spectroscopy are listed and compared with those of [Ga(DATA^{m})], [Ga(CyAAZTA)]$^{-}$, [Ga(AAZTA)]$^{-}$ and [Ga(NOTA)] in Table 1. (The experimental details, the definitions and equations used for the evaluation of the equilibrium data and the equilibrium characterization of Ca^{II}-, Zn^{II}-, Mn^{II}-, Cu^{II}- and Ln^{III}-complexes formed with **L1** and **L2** are summarized in ESI).

Table 1. Stability and protonation constants (log*K*) of [Ga(**L1**/**L2**)], [Ga(DATA^{m})], [Ga(CyAAZTA)], [Ga(AAZTA)] and [Ga(NOTA)] complexes (0.15 M NaCl, 25°C).

	GaL	Ga(HL)	Ga(H_2L)	Ga(L)OH	log$\beta_{Ga(L)OH}$
[Ga(L1)]	**18.77(3)**	2.41(3)	–	4.04 (4)	**14.74 (4)**
[Ga(L2)]	**21.70(4)**	2.51(3)	–	3.75 (3)	**17.94 (3)**
[Ga(DATA^{m})][a]	**21.54**	2.42	–	6.25	**15.29**
[Ga(CyAAZTA)]$^{-}$[b]	**21.39**	4.09	2.32	7.31	**14.08**
[Ga(AAZTA)]$^{-}$[c]	**21.15**	3.14	1.14	4.60	**16.57**
[Ga(NOTA)][d]	**29.60**	0.9	–	9.83	**19.77**

[a] Ref. [17]. [b] Ref. [21]. [c] Ref. [9]. [d] Ref. [26] (0.1M TMACl, 298K).

The stability constants of Ga^{III}-complex formed with **L2** is higher by 3 log*K* units than that of **L1**, which might be explained by the higher total basicity of **L2** (ΣlogK_i^H, Table S3) and their different structural properties. The logK_{GaL} values of Ga(**L2**) is similar to those of [Ga(DATA^{m})], [Ga(CyAAZTA)]$^{-}$ and [Ga(AAZTA)]$^{-}$. In Ga^{III}-complexes formed with **L1**/**L2**, the Ga^{III} ion is coordinated by three N and three O donor atoms. However, the structure of the pre-organised coordination cage formed by the donor atoms in **L1**/**L2** is clearly influenced by the rigidity of the fused heterobicyclic skeleton. By considering the logK_{GaL} values of **L1**/**L2**, it can be assumed that the coordination cage of **L2** provides a significantly favourable coordination environment for the Ga^{III}-ion in the corresponding complex. Interestingly, the formation of [Ga(**L1**)OH]$^{-}$ and [Ga(**L2**)OH]$^{-}$ species (log$K_{Ga(L)OH}$, Table 1) occurs at notably lower pH values than that of [Ga(AAZTA)OH]$^{2-}$, [Ga(DATA^{5m})OH]$^{-}$, [Ga(CyAAZTA)OH]$^{2-}$ and [Ga(NOTA)]. A comparison of the log$\beta_{Ga(L)OH}$ values of the [Ga(L)OH] species predominant at physiological conditions shows that [Ga(**L2**)OH]$^{-}$ is characterized by the highest cumulative stability constant among the Ga^{III}-complexes formed with AAZTA derivatives. The equilibrium data obtained by the pH-potentiometric titration have been used to calculate the species distribution diagram for the Ga^{III}-**L1** and Ga^{III}-**L2** systems (Fig. 3 and 4). Amount of Ga^{III}_{aq}, [Ga(OH)$_4$] and Ga(L)OH species achieved by ^{1}H- and ^{71}Ga-NMR studies of the Ga^{III}-**L1** and Ga^{III}-**L2** systems are also shown in Fig. 3 and 4.

The species distribution diagrams, the ^{1}H- and ^{71}Ga-NMR spectra (Fig. 3, 4, S7-S10) indicate that the complex formation is complete for [Ga(**L1**)] and [Ga(**L2**)] at pH≥2.0 and pH≥1.5, respectively. The ^{71}Ga-NMR signal of the highly symmetric $[Ga(H_2O)_6]^{3+}$ species is relatively sharp at -log[H^{+}]= 0.0 in the Ga^{III} -**L1** and Ga^{III}-**L2** systems (Fig. S7 and S9, $\nu_{½}$ = 55 Hz). The intensity of the ^{71}Ga-NMR signals decreases by increasing the pH due to the formation of protonated [Ga(H**L1**)]$^{+}$ and [Ga(H**L2**)]$^{+}$ species in the -log[H^{+}] ranges 1-2 and 0.5-1.5, respectively. In the pH range of 2-3, the deprotonation of the [Ga(HL)]$^{+}$ species results in a slight upfield shift of all ^{1}H-NMR signals which might be explained by the fact that the protonation of [Ga(**L1**/**L2**)] complexes takes place at the weakly coordinated carboxylate group of the ligand.

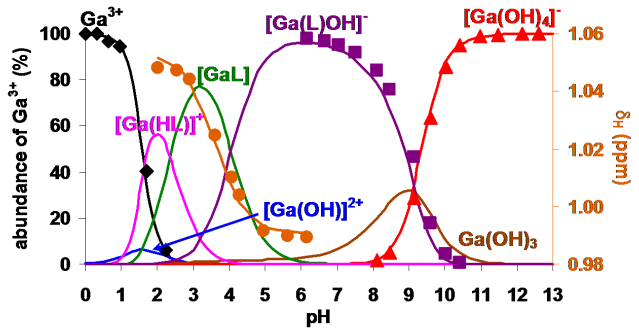

Figure 3. The percentage of the Ga^{3+}_{aq} (◆), $[Ga(L)OH]^-$ (■) and $[Ga(OH)_4]^-$ (▲) vs. pH calculated from the ^{1}H- and ^{71}Ga-NMR spectra of the Ga^{III}-**L1** system. Chemical shift of the -CH_3 protons (●) as a function of pH. The species distribution was calculated from the equilibrium data (Tables 1 and S3) obtained by pH-potentiometric titration ([Ga^{3+}] = [**L1**] = 10.0 mM, 0.15 M NaCl, 25°C).

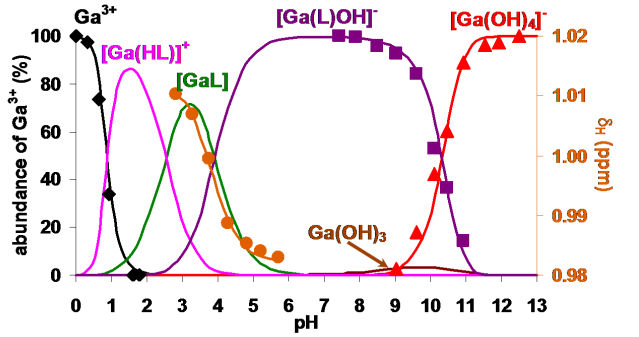

Figure 4. The percentage of the Ga^{3+}_{aq} (◆), $[Ga(L)OH]^-$ (■) and $[Ga(OH)_4]^-$ (▲) vs. pH calculated from the ^{1}H- and ^{71}Ga-NMR spectra of the Ga^{III}-**L2** system. Chemical shift of the –CH_3 protons (●) as a function of pH. The species distribution was calculated from the equilibrium data (Tables 1 and S3) obtained by pH-potentiometric titration ([Ga^{3+}] = [**L2**] = 10.0 mM, 0.15 M NaCl, 25°C).

Generally the line-width of ^{71}Ga-NMR signals (^{71}Ga is quadrupolar nucleus) is strongly influenced by the symmetry of Ga^{III}-complexes ([Ga(DATA^m)]: δ_{Ga}=129 ppm, $\nu_{½}$ = 1000 Hz; $[Ga(CyAAZTA)]^-$: δ_{Ga}=119 ppm, $\nu_{½}$ = 4700 Hz, 308 K and $[Ga(AAZTA)]^-$: δ_{Ga}=118 ppm, $\nu_{½}$ = 2200 Hz).[9,17,21] Moreover, the broadening or sharpening of the ^{71}Ga-NMR signal could be interpreted by the interaction of the nuclear quadrupole moment with the electric-field gradient at the ^{71}Ga nucleus.[27] At pH=3.5, the ^{71}Ga-NMR signals of [Ga(**L1**/**L2**)] complexes are very broad and not observable, as a result of the asymmetric coordination environment of the Ga^{3+} ion provided by the rigid structure of **L1**/**L2** (Fig. S8 and S10). At pH>3.0 the formation of the $[Ga(L)OH]^-$ species is evidenced by the extra equivalent base consumption during the pH-potentiometric titration and the shift of all the signals to lower frequency in the ^{1}H-NMR spectrum (Fig. S8 and S10). In the pH range 6-8, the $[Ga(L)OH]^-$ species predominates in both Ga^{III}-**L1** and Ga^{III}-**L2** systems. Since the ^{1}H-NMR spectra of the [Ga(**L1**)OH]$^-$ and [Ga(**L2**)OH]$^-$ contain several broad multiplets, it can be assumed that the $[Ga(L)OH]^-$ species of both Ga^{III} complexes are quite rigid structures. In the [Ga(**L1**)OH]$^-$ and [Ga(**L2**)OH]$^-$ species the Ga^{III} ion is presumably coordinated by three N, two exocyclic carboxylate O donor atoms and the OH^- ion (the acetate pendant arm located on the endocyclic nitrogen atom does not participate in the coordination of the Ga^{III} ion, see DFT calculations below). At pH>8.5, the competition of **L1**/**L2** with OH^- ion for Ga^{III} takes place by the appearance of the ^{71}Ga-NMR signal of the $[Ga(OH)_4]^-$ (δ_{Ga}=223 ppm, $\nu_{½}$ = 90 Hz, Fig. S8 and S10) and by the ^{1}H-NMR signals of the free **L1**/**L2** ligands.

The intensity of the ^{71}Ga-NMR signal of the $[Ga(OH^-)_4]^-$ species increases by increasing pH due to the dissociation of [Ga(**L1**)OH]$^-$ and [Ga(**L2**)OH]$^-$ species in the pH ranges 7.5-10.5 and 9.0-11.5, respectively. In the Ga^{III}-**L1** system, the $Ga(OH)_3$ species is formed in relatively large quantity due to the low stability of the [Ga(**L1**)OH]$^-$ species. The ^{1}H-NMR signal of the CH_3- protons of free and complexed **L1**/**L2** are well separated with chemical shifts of 0.8 and 1.0 ppm, respectively. The deprotonation of the free **L1**/**L2** ligands results in a significant upfield shift of CH_3- protons, whereas the frequency of CH_3 protons in [Ga(**L1**)OH]$^-$ and [Ga(**L2**)OH]$^-$ species remains unchanged. The intensity of the CH_3- protons of the Ga(**L1**/**L2**) complexes decreases with the increase of pH due to the dissociation of the [Ga(**L1**/**L2**)OH]$^-$ species and the formation of the $[Ga(OH)_4]^-$ (Fig. S8 and S10). The stability and protonation constant of Ga(**L1**) and Ga(**L2**) complexes obtained by the pH-potentiometry and multinuclear NMR spectroscopy) are in very good agreement (Table S5).

Dissociation kinetics in solution

To evaluate the potential application of [Ga(**L1**/**L2**)] complexes as ^{68}Ga based radiodiagnostics for PET imaging, their kinetic inertness must be assessed, because the high kinetic inertness of the ^{68}Ga complexes is especially important for targeting purposes to guarantee the delivery of the radioisotope in the form of intact complex to the target organ or tissue. The Ga^{III}-complexes are generally characterized by high thermodynamic stability. Then, their kinetic properties are often measured in strong acidic ([H+]>1.0 M) and basic conditions ([OH-]>0.1 M).[26-28]

Generally, the base catalysed dissociation of Ga^{III}-complex is significantly faster than that of acid catalysed processes due to the hydrolytic properties of Ga^{III}-ion.[26-28] However, the conditions of such studies differ considerably from the physiological ones and the use of the results obtained in these experiments to predict the behaviour of Ga^{III} complexes in body fluids can be quite risky. Body fluids are very complex media, i.e. endogenous metal ions and ligands may exchange with the components of the administered ^{68}Ga complexes in transmetallation or transchelation reactions. The possibility of ^{68}Ga releasing after in vivo administration of the complex, is determined by thermodynamic relations, expressed by the stability constants of the different complexes formed in body fluids. Based on the equilibrium data (Tables 1, S3, S4), the endogenous metal ions (mainly Cu^{II} and Zn^{II}) or serum proteins such as transferrin may compete with [Ga(L1/L2)] complexes resulting in the dissociation of the latter. On these premises, the

transmetallation and transchelation reactions with Cu^{II} and transferrin have been studied by spectrophotometry close to physiological conditions for the [Ga(L1/L2)] complexes.

Transmetallation reactions occurring between [Ga(**L1**/**L2**)] complexes and Cu^{II} ions have been investigated by spectrophotometry at high [Ga(**L1**/**L2**)] excess ($[GaL]_{tot}/[Cu^{II}]_{tot}$ = 10 and 20) in the presence of citrate to prevent the hydrolysis of the released Ga^{III} and the exchanging Cu^{II} ions in the pH range 6.0-9.0. The k_d pseudo-first-order rate constants characterizing the transmetallation reactions of Ga(**L1**/**L2**) complexes (Fig. S13) indicate that the rate of the transmetallation reaction is directly proportional to the OH^- concentration but does not depend on [Cu^{II}]. Accordingly, the reactions occur through the spontaneous (k_0) and the OH^--ion assisted (k_{OH}) dissociation of the dominant [Ga(**L1**))OH]$^-$ and [Ga(**L2**)OH]$^-$ species (Scheme 2), followed by a fast reaction between the released **L1**/**L2** ligand and the free Cu^{II} ions. However, the k_d vs. [OH^-] curve for [Ga(**L1**)OH]$^-$ is a saturation curve (Fig. S13), which can be interpreted by assuming the formation of the di-hydroxo $[Ga(\mathbf{L1})(OH)_2]^{2-}$ intermediate characterized by the $K_{Ga(L)(OH)2}$ equilibrium constants. Unfortunately, the results of the equilibrium studies (pH-potentiometry, ^{1}H and ^{71}Ga-NMR) could not confirm the formation of the $[Ga(\mathbf{L1})(OH)_2]^{2-}$ intermediate, which might be characterized by a very low kinetic inertness due to the coordination of only 4 donor atoms of the ligand to the Ga^{III} ion. By taking into account these considerations, the spontaneous dissociation of the $[Ga(\mathbf{L1})(OH)_2]^{2-}$ intermediate is more probable, characterized by the k_{OH}^2 rate constants. The mechanisms of the transmetallation reactions for the [Ga(**L1**)OH]$^-$ and [Ga(**L2**)OH]$^-$ are summarized in Scheme 2.

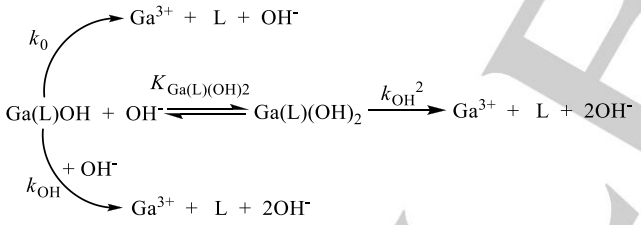

Scheme 2. Proposed mechanism of the transmetallation reactions for the [Ga(**L1**)] and [Ga(**L2**)] complexes. The reaction path in the middle is valid for [Ga(**L1**)] complex only.

The rate and stability constants characterising the transmetallation reaction of [Ga(**L1**)] and [Ga(**L2**)] with Cu^{II} are listed and compared with those of [Ga(DATA^m)], [Ga(CyAAZTA)]$^-$ and [Ga(AAZTA)]$^-$ complexes in Table 2 (Experimental details, definitions and equations used for the evaluation of the kinetic data are summarized in ESI).

The rate constants summarized in Table 2 indicate that spontaneous (k_0) and OH^--assisted (k_{OH}) dissociation of [Ga(**L2**)OH]$^-$ is significantly slower than that of [Ga(**L1**)OH]$^-$ and [Ga(CyAAZTA)OH]$^{2-}$ complexes. Interestingly, the k_0 and k_{OH} rate constants of [Ga(**L2**)OH]$^-$ are one order of magnitude lower than the corresponding rate constant of [Ga(AAZTA)OH]$^{2-}$. The spontaneous dissociation of [Ga(**L1**/**L2**)OH]$^-$, [Ga(DATA^m)OH]$^-$, [Ga(CyAAZTA)OH]$^{2-}$ and [Ga(AAZTA)OH]$^{2-}$ presumably occurs by the intramolecular rearrangement of the Ga^{III}-complexes with the stepwise de-coordination of each donor atom and consequent release of the Ga^{III}-ion. The very slow spontaneous dissociation of [Ga(**L2**)OH]$^-$ can be ascribed to its configuration providing a favourable and rigid coordination environment for the Ga^{III}-ion, leading to slower intramolecular rearrangements and OH^- assisted dissociation processes. Using the rate and equilibrium constants presented in Table 2, the half-lives ($t_{1/2}$=ln2/k_d) of the dissociation reactions of [Ga(**L1**)OH]$^-$ and [Ga(**L2**)OH]$^-$ at pH=7.4 have been calculated and compared with that of [Ga(DATA^m)OH]$^-$, [Ga(CyAAZTA)OH]$^{2-}$ and [Ga(AAZTA)OH]$^{2-}$ complexes. The $t_{1/2}$ values of [Ga(**L1**)OH]$^-$, [Ga(**L2**)OH]$^-$, [Ga(DATA^m)OH]$^-$, [Ga(CyAAZTA)OH]$^{2-}$ and [Ga(AAZTA)OH]$^{2-}$ are 0.27, 295, 11.2, 8.5 and 21 hours, respectively, highlighting that [Ga(**L2**)OH]$^-$ is characterised by the highest kinetic inertness, due to a very slow spontaneous and OH^--assisted dissociation. The dissociation of the "gold standard" [Ga(NOTA)] is significantly slower (several weeks at pH>13)[27] than that of [Ga(**L2**)OH]$^-$. However, [Ga(**L2**)OH]$^-$ is characterized by the highest kinetic inertness among the Ga^{III}-complexes formed with AAZTA-like ligands.

Table 2. Rate (k) and equilibrium (K) constants and half-life values ($t_{1/2}$=ln2/k_d) characterizing the transmetallation and the transchelation reactions of [Ga(**L1**/**L2**)], [Ga(DATA^m)], [Ga(CyAAZTA)]$^-$ and [Ga(AAZTA)]$^-$ with Cu^{II} and transferrin (25°C)

	Ga(L1)	**Ga(L2)**	**Ga(DATA^m)[a]**	**Ga(CyAAZTA)[b]**	**Ga(AAZTA)[c]**
k_0 / s^{-1}	1.4±0.1 ·10^{-4}	4.3± 0.2 ·10^{-7}	8.0·10^{-6}	1.7·10^{-5}	3.0·10^{-6}
k_{OH} / $M^{-1}s^{-1}$	–	0.6±0.1	31	68	10
k_{OH^2} / $M^{-1}s^{-1}$	1.8± 0.2 ·10^{-3}	–	–	–	–
$K_{Ga(L)(OH)2}$ / M^{-1}	1.5± 0.3·10^6	–	–	–	–
k_d / s^{-1} (pH=7.4)	(7 ± 1) ·10^{-4}	(6.5±0.3) ·10^{-7}	1.7·10^{-5}	2.3·10^{-5}	9.2·10^{-6}
$t_{1/2}$ / h (pH=7.4)	**0.27±0.05**	**295±15**	**11.2**	**8.5**	**21**
$k_d \times 10^6$ s^{-1} (sTf exch.)[d]	650±50	0.7±0.1	21	29	8
$t_{1/2}$ / h (sTf exch.)[d]	**0.29**	**283**	**9.4**	**6.6**	**24**

[a] Ref. [17]. [b] Ref. [21] (0.1M KCl). [c] Ref. [9] (0.1M KCl). [d] 0.025M $NaHCO_3$, M NaCl, 25°C, pH = 7.4.

Transchelation reactions with human serum transferrin: It is well established that Ga^{III} is transported through the circulatory system by the serum iron transport protein transferrin due the relatively high concentration of transferrin in human plasma[29,30] and the strong affinity of Ga^{III} to transferrin (Ga^{III}-transferrin: logK_{GaTf}=18.9, logK_{Ga2Tf}=17.7).[31] Since human serum transferrin is normally 30% saturated with Fe^{III},[32] it has a relatively high

capacity to bind Ga^{III} and to compete with ligands for the Ga^{III}-ion, thus resulting in the *in vivo* dissociation of the dominant [Ga(**L1**)OH]$^-$ and [Ga(**L2**)OH]$^-$ species. To assess the extent of Ga^{III} release in the competition reactions of [Ga(**L1**)OH]$^-$ and [Ga(**L2**)OH]$^-$ with transferrin, the ligand exchange reactions between Ga^{III}-complexes and human serum transferrin (sTr) have been studied by spectrophotometry at the absorption band of the Ga^{III}-sTf complex in the 240-250 nm range. The rate constant (k_d) and half-life ($t_{1/2}$=ln2/k_d) values characterizing the trans-chelation reactions of [Ga(**L1**)OH]$^-$, [Ga(**L2**)OH]$^-$ and sTf are shown and compared with those of [Ga(DATA^m)], [Ga(CyAAZTA)]$^-$ and [Ga(AAZTA)OH]$^{2-}$ in Table 2. (Experimental details, definitions and equations used for the evaluation of the kinetic data are summarized in ESI).

The k_d rate constants obtained for the ligand exchange reaction of [Ga(**L1**)OH]$^-$, [Ga(**L2**)OH]$^-$ with sTf were found to be (650±50)×10^{-6} s^{-1} and (0.7±0.1) ×10^{-6} s^{-1}, which are essentially equal to those obtained in the metal exchange reaction between [Ga(**L1**)OH]$^-$, [Ga(**L2**)OH]$^-$ and Cu^{II} in the presence of citrate excess ([Ga(**L1**)OH]$^-$: k_d=720×10^{-6} s^{-1}; [Ga(**L2**)OH]$^-$: k_d=0.65×10^{-6} s^{-1}, 0.15 M NaCl, 25°C). These findings can be interpreted by assuming that sTf has practically no effect on the rate of the trans-chelation reactions, which has been controlled by the spontaneous and hydroxide assisted dissociation of [Ga(**L1**)OH]$^-$ and [Ga(**L2**)OH]$^-$ complexes followed by the fast reaction between the released Ga^{III}-ion and sTf. The comparison of the half-life ($t_{½}$) calculated for the Ga^{III}-complexes indicates that the kinetic inertness of [Ga(**L2**)OH]$^-$ is about 1000, 30, 43 and 13 times higher than those of the [Ga(**L1**)OH]$^-$, [Ga(DATA^m)], [Ga(CyAAZTA)]$^-$ and [Ga(AAZTA)OH]$^{2-}$ complexes, respectively.

DFT study

Aiming to rationalise the different stability constants and dissociation kinetics of the Ga^{III} complexes with **L1** and **L2**, we performed DFT calculations at the TPSSh/TZVP level (see computational details below). These calculations provided optimized geometries containing six-coordinated Ga^{III} ions, which are directly bound to the three nitrogen atoms of the ligand and three oxygen atoms of the carboxylate groups. The metal coordination environments in both **L1** and **L2** can be described as distorted octahedral. The triangular face defined by the three coordinated oxygen atoms defines an angle of 9.9° (**L1**) and 8.7° (**L2**) with the plane delineated by the three nitrogen atoms of the ligand. The mean twist angles of these two triangular faces (49.4±8.6° and 50.6±8.0° for **L1** and **L2**, respectively), reflect a certain degree of distortion from an octahedron (ideal value 60°) towards a trigonal prism (ideal value 0°). Analogous calculations performed for [Ga(NOTA)] evidence a more symmetrical coordination environment, with virtually parallel O_3 and N_3 planes and a twist angle of 46.7±0.0°. The Ga-N and Ga-O distances calculated for [Ga(NOTA)] are 2.135 and 1.943 Å, respectively. The Ga-N and Ga-O distances involving N2, N3, O1 and O2 in the **L1** and **L2** complexes are similar to those of obtained for [Ga(NOTA)] and [Ga(DATA^m)], while the Ga-N1 and Ga-O2 distances are considerably longer (Fig. 5, see also Table S6). These results suggest that the presence of the additional six-membered ring in the bicyclic scaffold of the ligand introduces some steric hindrance for the coordination of N1, causing a concomitant lengthening of the *trans* Ga-O2 distance. This effect is more pronounced in [Ga(**L1**)] than in [Ga(**L2**)], which explains the lower stability of the former. This is in line with the relative free energies obtained with DFT, which predict a higher stability of [Ga(**L2**)] by 7.5 kJ mol^{-1}. A more detailed analysis of the Ga^{III} coordination environment was carried out by calculating the electron density (ρ) at the bond critical points (BCPs), which can be correlated to the strength of the metal-donor bonds.[33] The results (Fig. 5 and Table S7) show that the Ga-O bonds are stronger than the Ga-N ones, as would be expected. The value of ρ_{BCP} calculated for the Gd-N1 bonds is lower for the complex of **L1**, confirming a weaker binding of N1 in [Ga(**L1**)] than in [Ga(**L2**)].

The ^{71}Ga NMR chemical shifts of [Ga(**L1**)] and [Ga(**L2**)] were calculated using relativistic DFT calculations (see computational details below) following a methodology similar to that employed recently to predict ^{89}Y NMR shifts.[34] To assess the accuracy of our calculations, we also computed the chemical shifts of [Ga(DATA^m)], [Ga(NOTA)] and [Ga(OH)$_4$]$^-$. For chemical shift calculation purposes we computed the isotropic ^{71}Ga nuclear shielding of [Ga(H$_2$O)$_6$]$^{3+}$, so that the systems chosen for ^{71}Ga NMR chemical shifts calculations cover a chemical shift range of 223 ppm (Table 3).

Table 3. Experimental ^{71}Ga NMR chemical shifts (δ^{exp}) and linewidths ($\nu_{½}$) , isotropic ^{71}Ga nuclear shielding values (σ_{iso}) and calculated ^{71}Ga NMR chemical shifts (δ^{calc}) obtained with relativistic DFT calculations.

Complex	δ^{exp} (ppm)	$\nu_{½}$ (Hz)	σ_{iso} (ppm)	δ^{calc} (ppm)
[Ga(H$_2$O)$_6$]$^{3+}$	0	150	1901.8	0
[Ga(**L1**)]	[a]	[a]	1782.5	119
[Ga(**L2**)]	119	20000	1779.3	122
[Ga(DATA^m)][b]	129	1000	1778.8	123
[Ga(NOTA)][c]	170	210	1741.1	161
[Ga(OH)$_4$]$^-$	223	90	1653.0	249

[a] Too broad to be observed. [b] Ref. [20]. [c] Ref. [27].

Initial test calculations indicated that the agreement between experimental and calculated ^{71}Ga NMR shifts improved considerably when explicit second sphere water molecules were included in the models of [Ga(OH)$_4$]$^-$ and [Ga(H$_2$O)$_6$]$^{3+}$. Thus, we performed calculations using a mixed cluster-continuum approach on the [Ga(OH)$_4$]$^-$·8H$_2$O and [Ga(H$_2$O)$_6$]$^{3+}$·12H$_2$O systems.[35]

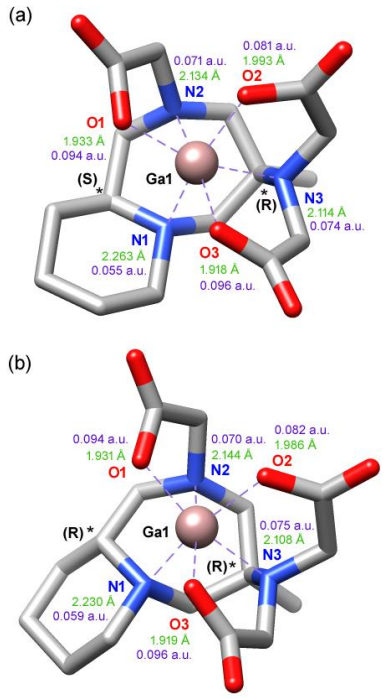

Figure 5. Geometries of the [Ga(**L1**)] (a) and [Ga(**L2**)] (b) complexes optimized at the TPSSh/TZVP level. Bond distances of the metal coordination environments and electron densities at the corresponding bond critical points are also provided.

Our DFT calculations provide ^{71}Ga NMR chemical shifts in good agreement with the experimental values, the largest deviation being observed for the $[Ga(OH)_4]^-$ complex. The chemical shift calculated for [Ga(**L2**)] (122 ppm) is in excellent agreement with the experimental value (119 ppm), which supports that our DFT calculations provide a good model of the structure of this complex in solution. The chemical shifts calculated for [Ga(**L1**)] and [Ga(**L2**)] are very similar, as would be expected given the very similar coordination environment of Ga^{III} in the two complexes. Geometry optimizations of the hydroxo complexes reveals that one of the carboxylate groups of the ligand remains uncoordinated, with a hydroxide anion completing the six-coordination environment around the metal ion. The [Ga(**L1**)(OH)]$^-$ and [Ga(**L2**)(OH)]$^-$ complexes present very similar bond distances of the metal coordination environment (Fig. S17). However, our DFT calculations provide a relative free energy of the [Ga(**L2**)OH]$^-$ species with respect to [Ga(**L1**)OH]$^-$ of -11.3 kJ mol^{-1}, reflecting again the ability of **L2** to form more stable Ga^{III} complexes.

Radiochemistry

The practical value of a given chelator for application in ^{68}Ga-PET radiopharmaceuticals is determined by two main aspects, namely, its resistance against dissociation of the radiometal in living organisms (sometimes referred to as "*in vivo* stability") which is directly linked to kinetic inertness, and the experimental conditions required for radiometal complexation (labelling). Regarding the latter, the necessity to produce radiopharmaceuticals with sufficiently high molar activity[36] requires efficient radiometal incorporation at the lowest possible chelator concentration. Furthermore, rapid complex formation at ambient temperature and physiological pH is an attractive feature, being indispensable for labelling of targeting vectors that do not tolerate elevated temperatures or challenging pH values, *e.g.* large proteins like antibodies, which is however of lesser relevance for the short-lived ^{68}Ga. More importantly, such properties would provide access to ^{68}Ga tracers *via* "shake-and-shoot" kits, that is, by simple addition of ^{68}Ge/^{68}Ga generator eluate to pre-conditioned vials containing lyophilized precursor and excipients, as known from ^{99m}Tc radiopharmaceuticals.[37]

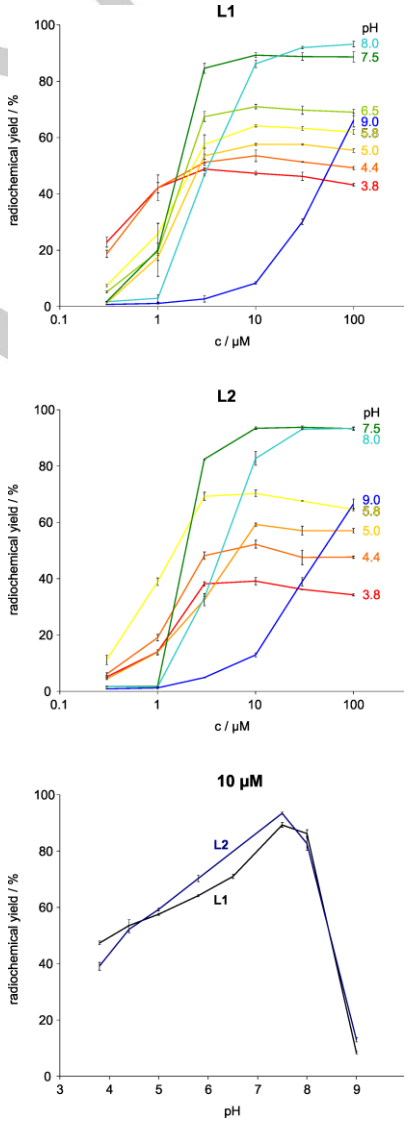

Figure 6. $^{68}Ga^{III}$-incorporation as functions of concentration for **L1** (a) and **L2** (b) for different pH values (reaction for 5 min at 25°C, mean values ± SD, n = 3; incorporation was determined by radio-TLC). At 10 µM ligand concentration, optimal labeling of both ligands is achieved at neutral to slightly basic pH (c).

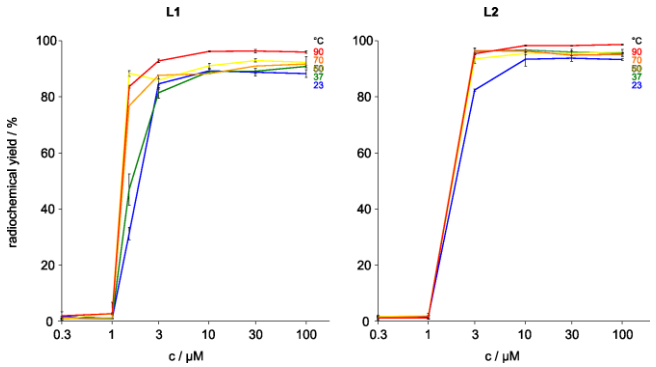

Figure 7. $^{68}Ga^{III}$-incorporation *vs* concentration for **L1** (left) and **L2** (right) at different temperatures (reaction for 5 min at pH 7.5, mean values ± SD, n = 3).

However, the cyclic polyaza-polycarboxylate chelators DOTA and NOTA, which are most frequently used in ^{68}Ga tracers, do not allow for labelling at neutral pH, single-digit µM concentration, and room temperature within a few minutes, while this was found to be feasible for several acyclic structures at slightly acidic pH[38] as well as for phosphinate-pendant triazacyclononanes at pH 3.[39,40] Against this background, it is remarkable that the optimal pH for labelling of PIDAZTA isomers **L1**/**L2** lies between 7 and 8 while at pH 7.5, nearly quantitative labelling (89.2% and 93.5% for **L1** and **L2**, respectively) at room temperature is achieved already at chelator concentrations below 10 µM (Fig. 6).

Notably, elevated temperatures have an almost negligible influence and do not substantially improve the labelling yield at lower concentrations, particularly for **L2** (Fig. 7). Such behaviour might be considered counterintuitive because it is fundamentally different from many established $^{68}Ga^{III}$ chelators, particularly those based on polyazacycloalkanes, which exhibit the corresponding pH-optimum at values around 3-4[39-41] and show a strong influence of temperature on the required chelator concentration (as a general rule, an approximately 30-times lower concentration is required to achieve the same radiolabelling yield at 95°C as compared to 25°C).[38] An explanation might be that formation of **L1**/**L2** complexes from $Ga_n(OH)_{3n}$ (the prevalent form of $^{68}Ga^{III}$ at neutral pH)[42] and the competing dehydration of this hydroxide,[43] yielding non-reactive, insoluble $[Ga(O)OH]_n$[44] ("colloidal ^{68}Ga"), are apparently accelerated to a comparable extent upon heating (Scheme 3; $dk_1/dT \approx dk_2/dT$), essentially resulting in similar labelling yields over a wide range of temperatures.

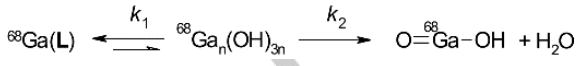

Scheme 3. Formation of $^{68}Ga(L)$, $^{68}Ga(OH)_3$ and $^{68}Ga(O)OH$ species.

Apart from minor quantitative deviations, both isomers nonetheless exhibit comparable overall labelling profiles. However, in accordance with kinetic data (Table 2), fundamental differences are observed in a transchelation challenge against aq. disodium EDTA. In order to enable observation over a larger time period, these experiments were conducted with the long-lived isotope ^{67}Ga ($t_{½}$ = 3.3 d) under physiological conditions (pH 7.4, 37 °C). Fig. 8 shows that in comparison to the parent structure $[^{67}Ga][Ga(AAZTA)]^-$, the annulated carbocycle causes a strong destabilisation for $[^{67}Ga][Ga(\mathbf{L1})OH]$ but results in a higher kinetic inertness of $[^{67}Ga][Ga(\mathbf{L2})OH]$.

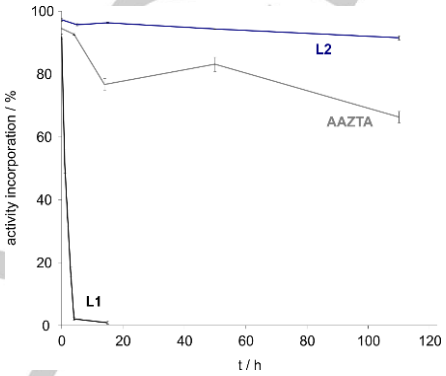

Figure 8. Percentage of intact $^{67}Ga^{III}$-complexes in 50 mM aq. disodium EDTA solution as functions of time (37°C, pH 7.4, mean values ± SD, n = 3).

In summary, the radiochemical investigations proved the suitability of **L2** for the elaboration of radiopharmaceuticals based on gallium isotopes, combining highly efficient labelling and strong resistance against demetallation at physiological conditions.

Experimental

1. Materials

$Ga(NO_3)_3$ was prepared by dissolving Ga_2O_3 (99.9%, Fluka) in 6M HNO_3 and evaporating of the excess acid. The solid $Ga(NO_3)_3$ was dissolved in 0.1 M HNO_3 solution. The concentration of the $Ga(NO_3)_3$ solution was determined by using standardised Na_2H_2EDTA in excess. The excess of Na_2H_2EDTA was measured with a standardized $ZnCl_2$ solution and xylenol orange as indicator. The concentration of $CaCl_2$ (Sigma), $MnCl_2$ (Sigma), $ZnCl_2$ (Sigma), $CuCl_2$ (Sigma) and $LnCl_3$ solutions were determined by complexometric titration with standardized Na_2H_2EDTA and xylenol orange ($ZnCl_2$ and $LnCl_3$), murexide ($CuCl_2$), *Patton & Reeder* ($CaCl_2$) and eriochrome black T ($MnCl_2$) as indicator. The H^+ concentration of the $Ga(NO_3)_3$ solution was determined by pH potentiometric titration in the presence of excess Na_2H_2EDTA.[9] The concentration of PIDAZTA isomers (**L1** and **L2**) and H_4AAZTA stock solutions was determined by pH-potentiometric titrations in the presence and absence of a 40-fold excess of Ca^{2+}. The citrate solution was prepared from $H_3Citrate$ (Sigma) and its concentration was determined by pH-potentiometry. The pH-potentiometric titrations were made with standardized 0.2 M NaOH.

2. Single Crystal X-Ray Diffraction Analysis

After careful inspection of the crystallization batches at the optical microscope, X-ray quality samples were selected, resulting in colorless needle-like prisms with dimensions of about 0.25 x 0.15 x 0.10 mm. The crystals of **3** and **L1** were mounted on a Bruker AXS APEXII CCD area-detector diffractometer, at room temperature, for the unit cell determination and data collection. Graphite-monochromatized MoKα (λ = 0.71073 Å) radiation was used with the generator working at 50 kV and 30 mA. Orientation matrixes were initially obtained from least-squares refinement on ca. 300 reflections measured in three different ω regions, in the range 0° < θ < 23°; cell parameters were optimized on the position, determined after integration, of ca. 8000 reflections. The intensity data were retrieved in the full sphere, within the θ limits reported in the cif files, from 1080 frames collected with a sample−detector distance fixed at 5.0 cm (50 s frame^{-1}; ω scan method, Δω = 0.5°). An empirical absorption correction was applied (SADABS).[45] Crystal structure was solved by direct methods using SHELXT2017 and refined with SHELXL-2017/1[46,47] within the Wingx suite of programs.[48] Hydrogen atoms were riding on their carbon atoms, for **3** and, for **L1**, were freely refined on their positions, derived from the difference Fourier map. Anisotropic temperature factors were assigned to all non-hydrogen atoms. Crystal data collection and refinement parameters are listed in the supporting information and in the *cif* files. A view of the molecules with the full numbering scheme is given in Fig. S1 and S3. Selected distances of bond lengths (Å) and angles (°) are given in Table S1 and S2, while atomic coordinates and displacement parameters are listed in the corresponding *cif* file.

CCDC numbers 1872753 and 1872767 contain the full supplementary crystallographic data for this work. The latter can be obtained free of charge from the Cambridge Crystallographic Data Centre via www.ccdc.cam.ac.uk/data_request/cif.

*Crystal data for **3**:* $C_{17}H_{25}N_3O_2$, *fw* = 303.4 gmol^{-1}, monoclinic $P2_1/c$ (No. 14), a = 7.8915(4), b = 23.0741(13) and c = 9.3186(5) Å, β = 93.0160(10) °; V = 1694.47(16) Å^3 ; Z = 4; Mo-K_α λ = 0.71073 Å; T (K) 293(2); ρ_{calc} = 1.189 g cm^{-3}, μ(Mo-K_α) = 0.079 mm^{-1}; θ range 1.765-26.439 °; data (unique), 3473 (2965); restraints, 0; parameters, 202; Goodness-of-Fit on F^2, 1.035; R_1 and wR_2 (I>2σ(I)), 0.0485 and 0.1203; R_1 and wR_2 (all data), 0.0555 and 0.1259; Largest Diff. Peak and Hole (e Å^{-3}), 0.246 and -0.186.

*Crystal data for **L1** (4R*,10aS*)-PDAZTA:* $C_{16}H_{27}N_3O_6$, *fw* = 357.4 gmol^{-1}, monoclinic $P2_1/c$ (No. 14), a = 9.8286(5), b = 7.9931(4) and c = 21.3905(10) Å, β = 93.1966(8) °; V = 1677.84(27) Å^3 ; Z = 4; Mo-K_α λ = 0.71073 Å; T (K) 293(2); ρ_{calc} = 1.415 g cm^{-3}, μ(Mo-K_α) = 0.108 mm^{-1}; θ range 1.907-26.525 °; data (unique), 3473 (2999); restraints, 0; parameters, 335; Goodness-of-Fit on F^2, 1.038; R_1 and wR_2 (I>2σ(I)), 0.0373 and 0.0957; R_1 and wR_2 (all data), 0.0434 and 0998; Largest Diff. Peak and Hole (e Å^{-3}), 0.249 and -0.174.

3. Equilibrium measurements

The protonation constants of **L1** and **L2**, and the stability and protonation constants of Ca^{II}-, Mn^{II}-, Zn^{II}- and Ln^{III}-complexes formed **L1** and **L2** were determined by pH-potentiometric titration from acidic to basic pH range. The metal-to-ligand concentration ratios were 1:1 (the concentrations of the ligands were generally 0.002 M). The stability and protonation constants of the "cold" Ga^{III}-**L1**/L**2** complexes were calculated from the pH-potentiometric titration of the Ga^{III}-L systems. The pH-potentiometric titrations of Ga^{III}-**L1** system were performed from acidic to basic and from basic to acidic pH range by studying the competition reaction between Ga^{III} and H^+ for **L1,** and **L1** and OH^- for Ga^{III}, respectively ([L]=[Ga^{III}]=2×10^{-3} M). Because of the high kinetic inertness, the stability and protonation constants of Ga(**L2**) were calculated from the pH-potentiometric data obtained from basic to acidic pH range, whereas the protonation constants of Ga(**L2**) were also evaluated from the pH-potentiometric titration achieved from acidic to basic pH range ([L]=[Ga^{III}]=2×10^{-3} M). The protonation constants of [Cu(**L1**)]$^-$ and [Cu(**L2**)]$^-$ were determined by pH-potentiometric titrations of CuL complex in the pH range of 1.7–11.7 ([CuL]=2×10^{-3} M). For pH measurements and pH-potentiometric titrations, a *Metrohm 785 DMP Titrino* titration workstation and a *Metrohm-6.0233.100* combined electrode were used. The pH potentiometric titrations were performed at constant ionic strength (0.15 M NaCl) in 6 mL samples at 25 °C. The solutions were stirred, and N_2 was bubbled through them. The titrations were made with 300 s waiting time in the pH range of 1.7-11.7. KH-phthalate (pH=4.005) and borax (pH=9.177) buffers were used to calibrate the pH meter. For the calculation of [H^+] from the measured pH values, the method proposed by *Irving et al.* was used.[49] A 0.01M HCl solution was titrated with the standardised NaOH solution in the presence of 0.15 M NaCl ionic strength. The differences between the measured (pH_{read}) and calculated pH (-log[H^+]) values were used to obtain the equilibrium H^+ concentration from the pH values, measured in the titration experiments. The ionic product of water (pK_w) at 25 °C in 0.15 M NaCl was found to be 13.83. The stability constant of [Cu(**L1**)]$^-$ and [Cu(**L2**)]$^-$ was determined by spectrophotometry in the [H^+] range of 0.01-1.0 M ([L]=[Cu^{2+}]=1×10^{-3} M). Seven samples were prepared and the H^+ concentration ([H^+]=0.010, 0.025, 0.050, 0.10, 0.35, 0.60 and 1.0 M) in the samples was adjusted with the addition of calculated amounts of 2.0 M HCl. The samples were kept at 25 °C for 7 days in order to attain the equilibrium (the time needed to reach the equilibrium was determined by spectrophotometry). The absorbance values of the samples were measured at 11 wavelengths (575, 595, 615, 635, 655, 675, 695, 715, 735, 755 and 775 nm). The ionic strength of samples with [H^+]=0.32, 0.60 and 1.0 M was not constant (the ionic strength of samples with [H^+]=0.010, 0.025, 0.050, 0.10 M was [H^+]+[Na^+]=0.15 M). For the equilibrium calculations, the molar absorptivities of the Cu^{II}, CuL, CuHL and CuH_2L species were used. The molar absorptivities of Cu^{II}, [Cu(**L1**)]$^-$ and [Cu(**L2**)]$^-$ complexes were determined by recording the Vis spectra (λ=400-800 nm) of 1.0×10^{-4}, 2.0×10^{-4}, 3.0×10^{-4} and 4.0×10^{-4} M solutions in the pH range 1.7-7.0 (0.15 M NaCl, 25 °C). The pH was adjusted by stepwise addition of concentrated NaOH or HCl. The spectrophotometric measurements were made with a *Cary 1E* spectrophotometer at 25 °C, using 1.0 cm cells. The

protonation and stability constants were calculated with the PSEQUAD program.[50]

4. NMR experiments

^{1}H- and ^{71}Ga-NMR measurement were performed with a Bruker DRX 400 (9.4 T) instrument equipped with a Bruker VT-1000 thermocontroller and a BB inverse z gradient probe (5 mm). The formation and protonation/deprotonation processes of the [Ga(**L1**)] and [Ga(**L2**)] were followed from basic to acidic pH range at 298 K in 0.15 M NaCl. For these experiments, 9.3 mM and 9.5 mM solutions of the [Ga(**L1**)] and [Ga(**L2**)] complexes in H_2O were prepared, respectively (A capillary with D_2O was used for lock). The pH was adjusted with the addition of concentrated solutions of NaOH or HCl. Because of the metal exchange between the [Ga(**L1**)OH]$^-$ or [Ga(**L2**)OH]$^-$ and [Ga(OH)$_4$] and the ligand exchange between the complexes and the free ligand $^-$ were in the "slow exchange regime" on the actual NMR timescales, the calculation of the log$\beta_{Ga(L)OH}$ value of [Ga(**L1**)OH]$^-$ and [Ga(**L2**)OH]$^-$ was performed by using the intensities of the ^{71}Ga-NMR signal of [Ga(OH)$_4$]$^-$ complex and the ^{1}H-NMR signal of the –C**H$_3$** protons in [Ga(**L1**)OH]$^-$ and [Ga(**L2**)OH]$^-$. The molar intensity values of ^{71}Ga-NMR signal of [Ga(OH)$_4$]$^-$ complex and the ^{1}H-NMR signal of the –C**H$_3$** protons in [Ga(**L1**)OH]$^-$ and [Ga(**L2**)OH]$^-$ complexes were determined by recording the ^{1}H-NMR spectra of 0.01, 0.015, 0.02 and 0.025 M solutions of [Ga(**L1**)OH]$^-$ and [Ga(**L2**)OH]$^-$ complexes at pH=6.0 and ^{71}Ga-NMR spectra of 0.01, 0.015, 0.02 and 0.025 M solutions of [Ga(OH)$_4$]$^-$ at pH=12.5 (0.15 M NaCl, 25 °C). The formation of [Ga(**L1**)] and [Ga(**L2**)] complexes were also studied by ^{1}H- and ^{71}Ga-NMR spectroscopy in the [H$^+$] range 0.01-1.00 M. In these experiments, 6+6 samples were prepared ([H$^+$]=0.01, 0.03, 0.13, 0.25, 0.50 and 1.0 M) for [Ga(**L1**)] and [Ga(**L2**)] complexes in H_2O (a capillary with D_2O was used for lock). The concentrations of [Ga(**L1**)] and [Ga(**L2**)] complexes were 9.3 mM and 9.5 mM. The [H$^+$] was adjusted with the addition of calculated amounts of 2.0 M HCl. The samples were kept at 25 °C for 7 days in order to attain the equilibrium. The ionic strength of samples with [H$^+$]=0.25, 0.50 and 1.0 M was not constant (the ionic strength of samples with [H$^+$]=0.01, 0.03 and 0.13 M was [H$^+$]+[Na$^+$]=0.15 M). Because of the metal exchange between the [Ga(**L1**)] and [Ga(**L2**)] and the free Ga^{III} ion was in the "slow exchange regime" on the actual NMR timescale, the calculation of the logK_{GaL} value of [Ga(**L1**)] and [Ga(**L2**)] was also performed with the use of the ^{71}Ga-NMR intensities of Ga^{III} ion by taking into account the protonation constants of the [Ga(**L1**)] and [Ga(**L2**)] complexes. The molar intensity value of ^{71}Ga-NMR signal of Ga^{III} ion was determined by recording the ^{71}Ga-NMR spectra of 0.01, 0.015, 0.02 and 0.025 M solutions of Ga^{III} in the presence of 1.0 M HNO_3. Calculation of the logK_{GaL} and log$\beta_{Ga(L)OH}$ values was performed by using the integral-[H$^+$] data pairs with the PSEQUAD program.[50]

5. Trans-metallation reactions

The rates of the exchange reactions taking place between [Ga(**L1**)], [Ga(**L2**)] and Cu^{II} in the presence of citrate were studied by spectrophotometry, following the formation of the [Cu(**L1**)]$^-$ and [Cu(**L2**)]$^-$ complexes at 300 nm, with the use of 1.0 cm cells and a Cary 1E spectrophotometer. The concentration of Cu^{II} was 0.1 and 0.2 mM, while that of Ga^{III}-complexes were 10 and 20 times higher, to ensure pseudo-first-order conditions. In order to prevent the hydrolysis of Ga^{III} and Cu^{II} ions, the transmetallation reactions were studied in the presence of citrate excess ([Cit]$_t$=2.0 mM). The exchange rates were studied in the pH range about 6.0-9.0. For keeping the pH values constant, MES (pH range 6.0-7.0), HEPES (pH range 7.0-8.5) and piperazine (pH range 8.5-9.0) buffers (0.01 M) were used. The temperature was maintained at 25 °C and the ionic strength of the solutions was kept constant (0.15 M NaCl). The pseudo-first-order rate constants (k_d) were calculated from the slope of the absorbance vs. time curves (ΔAbs/Δt) with Eq. 10 in Supporting Information. For the calculations, the molar absorptivities of [Cu(**L1**)]$^-$, [Cu(**L2**)]$^-$ and Cu(Cit)H$_{-1}$ were used, which were determined at 300 nm by recording the spectra of 1.0×10^{-4}, 2.0×10^{-4}, 3.0×10^{-4} and 4.0×10^{-4} M solutions in the pH range 5-10 (0.15M NaCl, 25°C). The calculations were performed with the use of the computer program *Micromath Scientist*, version 2.0 (Salt Lake City, UT, USA).

6. Trans-chelation reactions with human serum transferrin

The ligand exchange reaction between [Ga(**L1**)OH]$^-$, [Ga(**L2**)OH]$^-$ and human serum transferrin (Sigma, partially Fe^{III}-saturated) have been studied by spectrophotometry, following the formation of Ga(sTf) complex at 246 nm and pH=7.4 with the use of 1.0 cm cells and Cary 1E spectrophotometer. The concentration of the human serum transferrin solution was determined from the absorbance at 280 nm using the molar absorptivity ε_{280}=91200 cm^{-1}M^{-1}.[51] In order to ensure the pseudo-first-order condition, the rate of the ligand exchange reactions were studied in the presence of high excess of Ga^{III}-complexes ([Ga(**L1**)OH]$^-$=[Ga(**L2**)OH]$^-$=0.1 and 0.2 mM, [sTf]=10 μM)). The temperature was maintained at 25°C, the ionic strength and the hydrogen-carbonate concentration of the samples were kept constant; 0.15 M for NaCl and 0.025 M for $NaHCO_3$, respectively.

7. Computational details

Geometry optimizations of the [Ga(**L1**)], [Ga(**L2**)], [Ga(**L1**)OH]$^-$ and [Ga(**L2**)(OH)]$^-$ systems were performed using DFT calculations at the TPSSh/TZVP[52,53] level with the Gaussian 09 package (Revision D.01).[54] Solvent effects (water) were included by using the polarizable continuum model (PCM), in which the solute cavity is built as an envelope of spheres centered on atoms or atomic groups with appropriate radii. Specifically, we used the integral equation formalism variant of the polarizable continuum model (IEFPCM) as implemented in Gaussian 09.[55] No symmetry constraints were imposed during the optimizations. The stationary points found on the potential energy surfaces as a result of geometry optimizations were confirmed to correspond to energy minima rather than saddle points using frequency calculations. Wave function analysis was carried out by computing the electron density (ρ) at the bond critical points (BCP) with the computer program Multiwnf 3.2.[56] Geometry optimizations of the systems [Ga(H$_2$O)$_6$]$^{3+}$·12H$_2$O, [Ga(OH)$_4$]$^-$·8H$_2$O, [Ga(NOTA)] and [Ga(DATA^m)] and subsequent frequency calculations were performed using the same methodology.

The calculations of the ^{71}Ga NMR shielding tensors were carried out using the ORCA program package (Version 3.0.1)[57]

using the TPSSh functional and the own nucleus as the gauche origin. Relativistic effects were included with the second order Douglas-Kroll-Hess (DKH2) method[58,59] in combination with the all-electron scalar relativistic TZVPPP-DKH basis set.[60] The RIJCOSX approximation[61-64] was used to accelerate the calculations with the aid of the Def2-TZVPP/JK[65] auxiliary basis set. The SCF convergence tolerances and integration accuracies of the calculations were increased from the defaults using the available TightSCF and Grid5 options (Grid7 for Ga). Solvent effects (water) were considered by using the COSMO solvation model as implemented in ORCA.[66] Chemical shifts were calculated as $\delta = (\sigma_{iso}^{ref} - \sigma_{iso})$ using $[Ga(H_2O)_6]^{3+}\cdot 12H_2O$ as a reference. The σ_{iso} values can be broken down into the diamagnetic (σ^d) and paramagnetic (σ^p) contributions, which provide shielding and deshielding contributions, respectively (Table S7).[67,68]

8. Radiochemistry

A $^{68}Ge/^{68}Ga$-generator with SnO_2 matrix (obtained from ITHEMBA LABS, South Africa) was eluted with 1.0 M aq. HCl. A fraction of 1.25 mL containing the highest activity (ca. 400 MBq) was mixed with a solution of HEPES (2 M; 0,800 µL) or sodium-acetate (4 M; 0.8 µL). From this solution aliquots of 90 µL (containing about 15 MBq or 0.15 pmol each) were transferred into eppendorf cups. 10 µL of stock solutions of the ligand (ranging 0.3 µM – 100 µM) were added and mixed well. Heating (if applied) was performed by placing the closed eppendorf vials into a thermostated water bath. After heating, labeling reactions were interrupted by placing the cups into a cold-water bath. Samples were analyzed by TLC (1.0 M NH_4OAc/MeOH (1:1) as mobile phase, where insoluble colloidal $^{68}Ga^{III}$ stays at the origin (R_F = 0) and the radiolabeled product is eluted with the solvent front (R_F = 0.5-0.6). The adjustment of different pH values for assessment of pH-dependence was completed with further addition of 1 M aq. NaOH or 1 M aq. HCl to the labelling solution prior to addition of the ligands. Synthesis of ^{67}Ga complexes was performed likewise, using ^{67}Ga in 0.05 M HCl (obtained from Mallinckrodt, Petten, The Netherlands) instead of ^{68}Ga.

Stabilities of the [^{67}Ga][GaL] complexes were tested by adding 100 µL (1 mM) of the product to 900 µL of 100 mM EDTA solution, followed by incubation at 25 °C for 5 d. Percentages of intact complexes were quantified using radio-TLC, by withdrawing samples (2.5 µL) during the reaction at 30, 60 and 90 min and spotting onto the TLC strip.

Conclusions

A conformational locking of mesocyclic diazepine-type chelators was achieved by the annulation of an additional six-membered saturated carbocycle to the 6-amino-1,4-diazepane moiety. Since the fused piperidine cycle encompasses one of the ring nitrogens, the resulting **pi**peridino[1,2-a]**diaz**epine-**t**riacetic **a**cid (PIDAZTA) ligands possess one acetic acid pendant arm less than the AAZTA parent structure. The structural modification furthermore gives rise to two distinct diastereomers, (4*R**,10a*R**)- and (4*R**,10a*S**)-PIDAZTA. The stereochemistry has a substantial effect on the thermodynamic stability and kinetic inertness of the Ga^{III}-complexes and entails notable differences in terms of radiochemistry. Unlike the radiogallium complexes of AAZTA and the (4*R**,10a*R**)-isomer, the latter of which particularly rapidly decomposes in a transchelation challenge vs EDTA, the (4*R**,10a*S**)-isomer does not show any substantial release of the radiometal under these conditions.

However, both isomers quantitatively incorporate $^{68}Ga^{III}$ within minutes at room temperature and chelator concentrations below 10 µM. This occurs most effectively at pH values between 7 and 8. PIDAZTAs are therefore the first chelators reaching their optimal labeling performance at truly physiological conditions. The demetallation-resistant isomer, (4*R**,10a*S**)-PIDAZTA, is therefore perfectly suited for use in combination with thermo- or acid-sensitive biomolecules. However, more importantly, PIDAZTA-based compounds appear ideal for application in ^{68}Ga-labelling kits. This is because the labeling reaction can be carried out at physiological pH (7.4) which is demanded for parenteralia in most pharmacopoeia documents, thus obviating addition of buffers after labelling or making compromises in terms of product specification. It is anticipated that clinical preparation of ^{68}Ga radiopharmaceuticals will be dominated by labeling kits in the near future. One such kit, Somatokit-TOC©, has received a marketing authorisation recently, and many more are currently in the approval pipeline of several companies. Hence, we conclude that PIDAZTA represents a valuable building block for future development of advanced ^{68}Ga radio-pharmaceuticals.

Acknowledgements

Authors C. P.-I and D. E.-G. thank Centro de Supercomputación de Galicia (CESGA) for providing the computer facilities. VC thanks Prof. A. Sironi for fruitful discussions and University of Milan for partial funding (PSR2018). Authors are grateful for the support granted by the Hungarian National Research, Development and Innovation Office (NKFIH K-128201 project). The research was also supported in a part by the EU and co-financed by the European Regional Development Fund under the projects GINOP-2.3.2-15-2016-00008 and GINOP-2.3.3-15-2016-00004.

Conflicts of interest

There are no conflicts of interest to declare.

Keywords: gallium • chelating agent • stability • thermodynamics • kinetics

[1] J. Notni, H.-J. Wester, *J. Label. Compd. Radiopharm.* **2018**, *61*, 141-153.

[2] F. Rösch, *Appl. Radiat. Isot.* **2013**, *76*, 24-30.

[3] I. Velikyan, *Molecules* **2015**, *20*, 12913-12943.

[4] E. W. Price, C. Orvig, *Chem. Soc. Rev.* **2014**, *43*, 260-290.

[5] P. Spang, C. Herrmann, F. Roesch, *Sem. Nucl. Med.* **2016**, *46*, 373-394.

[6] a) T. W. Price, J. Greenman, G. J. Stasiuk, *Dalton Trans.* **2016**, *45*, 15702-15724; b) J. Šimeček, O. Zemek, P. Hermann, J. Notni, H.-J. Wester, *Mol. Pharmaceutics* **2014**, *11*, 3893-3903; c) M. Eder, B. Wängler, S. Knackmuss, F. LeGall, M. Little, U. Haberkorn, W. Mier, M.

Eisenhut, *Eur. J. Nucl. Med. Mol. Imaging* **2008**, *35*, 1878-1886; d) M. T. Ma, C. Cullinane, C. Imberti C, J. Baguña Torres, S. Y. A. Terry, P. Roselt, R. J. Hicks, P. J. Blower, *Bioconjugate Chem.* **2016**, *27*, 309-318; e) C. Zhai, D. Summer, C. Rangger, H. Haas, R. Haubner, C. Decristoforo, *J. Label. Compd. Radiopharm.* **2015**, *58*, 209-214.

[7] G. J. Stasiuk, N. J. Long, *Chem. Commun.* **2013**, *49*, 2732-2746.

[8] S. Aime, L. Calabi, C. Cavallotti, E. Gianolio, G. B. Giovenzana, P. Losi, A. Maiocchi, G. Palmisano, M. Sisti, *Inorg Chem.* 2004, **43**, 7588-7590.

[9] Zs. Baranyai, F. Uggeri, A. Maiocchi, G. B. Giovenzana, C. Cavallotti, A. Takács, I. Tóth, I. Bányai, A. Bényei, E. Brucher, S. Aime, *Eur. J. Inorg. Chem.* **2013**, 147-162.

[10] G. Nagy, D. Szikra, Gy. Trencsényi, A. Fekete, I. Garai, A. M. Giani, R. Negri, N. Masciocchi, A. Maiocchi, F. Uggeri, I. Tóth, S. Aime, G. B. Giovenzana, Zs. Baranyai, *Angew. Chem. Int. Ed.* **2017**, *56*, 2118-2122.

[11] J. Seemann, B. Waldron, D. Parker, F. Roesch, *EJNMMI Radiopharm. Chem.* **2016**, *1*:4.

[12] J. Pfister, D. Summer, C. Rangger, M. Petrik, E. von Guggenberg, P. Minazzi, G. B. Giovenzana, L. Aloj, C. Decristoforo, *EJNMMI Res.* **2015**, *5*:74.

[13] L. Manzoni, L. Belvisi, D. Arosio, M. P. Bartolomeo, A. Bianchi, C. Brioschi, F. Buonsanti, C. Cabella, C. Casagrande, M. Civera, M. De Matteo, L. Fugazza, L. Lattuada, F. Maisano, L. Miragoli, C. Neira, M. Pilkington-Miksa, C. Scolastico, *ChemMedChem* **2012**, *7*, 1084-1093.

[14] Z. Wu, Z. Zha, S. R. Choi, K. Plössl, L. Zhu, H. F. Kung, *Nucl. Med. Biol.* **2016**, *43*, 360-371.

[15] B. P. Waldron, D. Parker, C. Burchardt, D. S. Yufit, M. Zimny, F. Roesch, *Chem. Commun.* **2013**, *49*, 579-581.

[16] J. Greiser, C. Kühnel, H. Görls, W. Weigand, M. Freesmeyer, *Dalton Trans.* **2018**, *47*, 9000-9007.

[17] E. Farkas, J. Nagel, B. P. Waldron, D. Parker, I. Tóth, E. Brucher, F. Rösch, Z. Baranyai, *Chem. Eur. J.* **2017**, *23*, 10358-10371.

[18] J. Seemann, B. P. Waldron, F. Roesch, D. Parker, *ChemMedChem* **2015**, *10*, 1019-1026.

[19] D. Parker, B. P. Waldron, *Org. Biomol. Chem.* **2013**, *11*, 2827-2838.

[20] D. Parker, B. P. Waldron, D. S. Yufit, *Dalton Trans.* **2013**, *42*, 8001-8008.

[21] A. Vágner, C. D'Alessandria, G. Gambino, M. Schwaiger, S. Aime, A. Maiocchi, I. Tóth, Zs. Baranyai, L. Tei, *ChemistrySelect* **2016**, *1*, 163-171.

[22] W. R. Harris, A. E. Martell, *Inorg. Chem.* **1976**, *15*, 713-720.

[23] R. J. Motekaitis, A. E. Martell, *Inorg. Chem.* **1980**, *19*, 1646-1651.

[24] A. S. Craig, D. Parker, H. Adams, N. A. Bailey, *J. Chem. Soc., Chem. Commun.* **1989**, 1793-1794.

[25] J.P.L. Cox, A.S. Craig, I.M. Helps, K.J. Jankowski, D. Parker, M.A.W. Eaton, A.T. Millican, K. Millar, N.R.A. Beeley, B.A. Boyce, *J. Chem. Soc., Perkin Trans I* **1990**, 2567-2576.

[26] J. Šimeček, M. Schulz, J. Notni, J. Plutnar, V. Kubíček, J. Havlíčková, P. Hermann, *Inorg. Chem.* **2012**, *51*, 577-590.

[27] C. J. Broan, J. P. L. Cox, A. S. Craig, R. Kataky, D. Parker, A. Harrison, A. M. Randall, G. Ferguson, *J. Chem. Soc. Perkin Trans. 2* **1991**, 87-99.

[28] V. Kubíček, J. Havlíčková, J. Kotek, G.Tircsó, P. Hermann, É. Tóth, I. Lukeš, *Inorg. Chem.* **2010** *49*, 10960-10969.

[29] G. E. Jackson, M. J. Byrne, *J. Nucl. Med.* **1996**, *37*, 379-386.

[30] P. M. May, P. W. Linder, D. R. Williams, *J. Chem. Soc. Dalton Trans.* **1977**, 588-595.

[31] W. R. Harris, V. L. Pecoraro, *Biochemistry* **1983**, *22*, 292-299.

[32] P. Aisen, A. Leibman, J. Zweier, *J. Biol. Chem.* **1978**, *253*, 1930-1937.

[33] M. Regueiro-Figueroa, C. Platas-Iglesias, *J. Phys. Chem. A* **2015**, *119*, 6436-6445.

[34] Y. Xing, A. K. Jindal, M. Regueiro-Figueroa, M. Le Fur, N. Kervarec, P. Zhao, Z. Kovacs, L. Valencia, P. Pérez-Lourido, R. Tripier, D. Esteban-Gómez, C. Platas-Iglesias, A. D. Sherry, *Chem. Eur. J.* **2016**, *22*, 16657-16667.

[35] D. Esteban-Gómez, C. Cassino, M. Botta, C. Platas-Iglesias, *RSC Adv.* **2014**, *4*, 7094-7103.

[36] I. Velikyan, G. J. Beyer, E. Bergström-Pettermann, P. Johansen, M. Bergström, B. Långström, *Nucl. Med. Biol.* **2008**, *35*, 529–536.

[37] D. Papagiannopoulou, *J Label Compd Radiopharm.* **2017**, *60*, 502-520.

[38] M. I. Tsionou, C. E. Knapp, C. A. Foley, C. R. Munteanu, A. Cakebread, C. Imberti, T. R. Eykyn, J. D. Young, B. M. Paterson, P. J. Blower, M. T. Ma, *RSC Adv.* **2017**, *7*, 49586-49599.

[39] G. Máté, J. Šimeček, M. Pniok, I. Kertész, J. Notni, H.-J. Wester, L. Galuska, P. Hermann. *Molecules* **2015**, *20*, 13112-13126.

[40] J. Notni, J. Šimeček, P. Hermann, H. J. Wester. *Chem. Eur. J.* **2011**, *17*, 14718-14722.

[41] G. Máté, D. Szikra, J. Šimeček, S. Szilágyi, G. Trencsényi, H. J. Wester, I. Kertész, L. Galuska, *J. Flow Chem.* **2016**, *6*, 86-93.

[42] B. Hacht, *Bull. Korean Chem. Soc.* **2008**, *29*, 372-376.

[43] H. Gamsjäger, P. Schindler, *Helv. Chim. Acta* **1967**, *50*, 2053-2057.

[44] M. Uchida, A. Okuwaki, *J. Sol. Chem.* **1998**, *27*, 965-978.

[45] G. M. Sheldrick, SADABS, Program for Absorption Correction; University of Göttingen, Göttingen, Germany, **1996**.

[46] G. M. Sheldrick, *Acta Crystallogr.* **2008**, *A64*, 112-122.

[47] G. M. Sheldrick, *Acta Crystallogr. C Struct. Chem.* **2015**, *71*, 3-8.

[48] L. J. Farrugia, *J. Appl. Cryst.* **2012**, *45*, 849-854.

[49] H. M. Irving, M. G. Miles, L. D. Pettit, *Anal. Chim. Acta* **1967**, *38*, 475-488.

[50] L. Zékány, I. Nagypál in '*Computational Method for Determination of Formation Constants*' Ed. D. J. Legett, Plenum, New York, **1985**, p. 291.

[51] H. Oe, H. N. Takahashi, E. Doi, M. Hirose, *J. Biochem*. **1989**, *106*, 858-863.

[52] J. Tao, J. P. Perdew, V. N. Staroverov, G. E. Scuseria, *Phys. Rev. Lett.* **2003**, *91*, 146401.

[53] A. Schäfer, C. Huber, R. Ahlrichs, *J. Chem. Phys.* **1994**, *100*, 5829.

[54] M. J. Frisch et al. Gaussian, Inc., Wallingford CT, **2009**.

[55] J. Tomasi, B. Mennucci, R. Cammi, *Chem. Rev.* **2005**, *105*, 2999-3093.

[56] T. Lu, F. Chen, *J. Comput. Chem.* **2012**, *33*, 580-592.

[57] F. Neese, The ORCA program system, *Wiley Interdiscip. Rev.: Comput. Mol. Sci.,* **2012**, *2*, 73.

[58] M. Barysz, A. J. Sadlej, *J. Mol. Struct. (Theochem)* **2001**, *573*, 181-200.

[59] M. Reiher, *Theor. Chem. Acc.* **2006**, *116*, 241-252.

[60] D. A. Pantazis, X.-Y. Chen, C. R. Landis, F. Neese, *J. Chem. Theory Comput.* **2008**, *4*, 908-919.

[61] F. Neese, F. Wennmohs, A. Hansen, U. Becker, *Chem. Phys.* **2009**, *356*, 98-109.

[62] R. Izsák, F. Neese, *J. Chem. Phys.* **2011**, *135*, 144105.

[63] T. Petrenko, S. Kossmann, F. Neese, *J. Chem. Phys.* **2011**, *134*, 054116.

[64] S. Kossmann, F. Neese, *Chem. Phys. Lett.* **2009**, *481*, 240-243.

[65] F. Weigend, R. Ahlrichs, *Phys. Chem. Chem. Phys.* **2005**, *7*, 3297-3305.

[66] S. Sinnecker, A. Rajendran, A. Klamt, M. Diedenhofen, F. Neese, *J. Phys. Chem. A* **2006**, *110*, 2235-2245.

[67] J. A. Platts, K. Gkionis, *Phys. Chem. Chem. Phys.* **2009**, *11*, 10331-10339.

[68] A. H. Greif, P. Hrobárik, V. Hrobárikova, A. V. Arbuznikov, J. Autschbach, M. Kaupp, *Inorg. Chem.* **2015**, *54*, 7199-7208.

10.1002/chem.201901512

WILEY-VCH

Entry for the Table of Contents (Please choose one layout)

Layout 2:

FULL PAPER

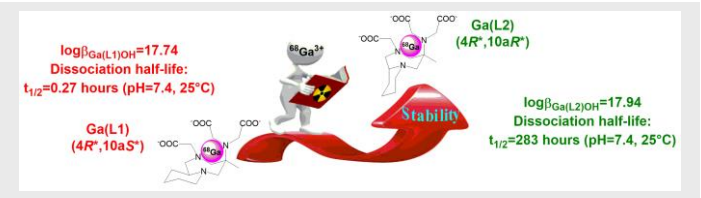

PIDAZTAs: bicyclic ligands for the development of ^{68}Ga-based radiopharmaceuticals. Quantitative radiolabelling in mild conditions in minutes and stereochemistry-driven thermodynamic and kinetic stability.

E. Farkas, A. Vágner, R. Negri, L. Lattuada, I. Tóth, V. Colombo, D. Esteban-Gómez, C. Platas-Iglesias, J. Notni, Zs. Baranyai,* G.B. Giovenzana**

Page No. – Page No.

PIDAZTA: Structurally Constrained Chelators for Efficient Formation of Stable Gallium-68 Complexes at Physiological pH